FACTA UNIVERSITATIS
Series:**Mechanical Engineering**
https://doi.org/10.22190/FUME210308050K

Original scientific paper

IRREVERSIBILITY ANALYSIS IN Al_2O_3-WATER NANOFLUID FLOW WITH VARIABLE PROPERTY

Krishan Kumar, Prathvi Raj Chauhan, Rajan Kumar, Rabinder Singh Bharj

Department of Mechanical Engineering,
Dr B R Ambedkar National Institute of Technology, Jalandhar, Punjab, India

Abstract. *The present numerical work deals with the optimization of the micro-channel heat sink using irreversibility analysis. The nanofluid of Al_2O_3-water with the different nanoparticles concentration and the temperature-dependent property is chosen as a coolant. The flow is considered as fully developed, steady, and laminar in the constant cross-section of circular channels. Navier-Stokes and energy equations are solved for a single-phase flow with total mass flow rate and heat flow rate as constant. The objective functions related to the frictional and heat transfer irreversibilities are framed to assess the performance of the micro-channel heat sink. The optimum channel diameter corresponding to the optimum number of channels is determined at the lowest total irreversibility for both constant property solution and variable property solution. Designed optimum diameter is observed maximum for 2.5% Al_2O_3-water nanofluid with $\mu(T)$ variation followed by 1% Al_2O_3-water nanofluid with $\mu(T)$ variation, 2.5% Al_2O_3-water nanofluid with constant property solution, and 1% Al_2O_3-water nanofluid with constant property solution.*

Key Words: *Micro-channel, Entropy Generation, Nanofluid, Property Variation*

1. INTRODUCTION

In recent times, the exponential rise is experienced in the capacity and loading related to the computing/transaction/processing/storage for information and communication technology applications (such as cloud computing, artificial intelligence, 5G, etc.). The electronic devices involved in such applications have high power consumption along with high heat generation [1]. This generated high heat flux needs to be managed efficiently. The micro-channel (MC) heat sinks with liquid cooling were found more advantageous

Received March 08, 2021 / Accepted June 18, 2021
Corresponding author: Rajan Kumar
Department of Mechanical Engineering, Dr BR Ambedkar National Institute of Technology, Jalandhar, Punjab 144011, India
E-mail: rajank@nitj.ac.in, rajan.rana9008@gmail.com

over conventional air cooling [2]. The cooling performance of these high-performance devices can be improved either by incrementing heat transfer (HT) surface area or by using a working fluid with excellent thermophysical properties. The fluids with better thermophysical properties can be prepared by synthesizing the base fluids with particles of nanometric size (1–100 nm) and termed as nanofluid (NF) [3, 4]. The thermal performance improves with the use of NF but more pumping power is required to move the fluid [5, 6]. Thus, the design and optimization of the thermal system consisting of the NF flow in the MC is an important concern for the research. The optimization of any thermal system can be assessed using entropy generation (EG), which is the measure of exergy loss of the system [7, 8]. It is always required to minimize the EG in any system for its better performance. The 2nd law analysis is important in understanding the EG and also a useful tool in designing and analyzing a thermal system with less entropy and loss of available work [9]. Bejan [10, 11] used the 1st and 2nd law of thermodynamics and provided a technique for minimizing the entropy generation rate for system optimization, which is known as the entropy generation minimization approach. Further, the effects of the thermophysical property variations in the case of micro-convective flows cannot be neglected because of the steeper temperature gradients [12].

Rastogi and Mahulikar [13, 14] implemented the theory of EG for the optimization of the MC heat sink with a laminar forced convection flow. The situation with minimum total EG rate results in the optimum channel diameter. Chauhan et al. [15] numerically optimized the MC heat sink using the EG minimization principle. No change in the temperature gradient in the axial direction was analyzed but an increase in the HT EG in the axial direction occurs because of the decrease in the temperature in the denominator when micro-dimensions were approached. Kumar et al. [16] performed numerical simulations to optimize the number of channels (N) corresponding to the channel diameter (D_N) at the micro-scale. At the microscale, frictional EG dominates over the HT EG due to an increase in the velocity gradient and a decrease in the temperature gradient in the radial direction.

Heshmatian and Bahiraei [17] analyzed the effects of viscosity gradient, Brownian diffusion, and shear rate on the irreversibility in the titanium dioxide (TiO_2)-water NF flowing through the circular MC. The total EG rate decreases with the enlargement of the nanoparticles because of the decrease in the frictional EG rate. Bianco et al. [18] used alumina (Al_2O_3) NF forced convective flow in a PV/T panel. The use of NF helped in the HT improvement which reduces the thermal EG. Also, the use of NF created more flow friction and resulted in a higher frictional EG. But due to the dominance of HT EG, the total EG was also less when NF was used as the working fluid. Manay et al. [19] experimentally investigated the EG in TiO_2-water NF flow through the MC heat sink with variable nanoparticles volume fraction (VF). The reduction in the height of the channel, as well as the introduction of the nanoparticles to the base fluid, resulted in the reduction of the thermal EG. Bianco et al. [20] performed a numerical study to analyze the irreversibility in the Al_2O_3 NF flow through a three-dimensional rectangular channel. The channel top wall was considered under a constant wall heat flux of 1000 W/m^2. The study found it convenient to use NFs because it helps in the reduction of the total irreversibility of the system. Alfaryjat et al. [21] studied EG in the NF flowing in a hexagonal MC heat sink. The numerical investigations were performed using Al_2O_3-water, copper oxide (CuO)-water, and silica (SiO_2)-water NF. The study concluded that with an increase in the Reynolds number (Re) and VF, a fall in the thermal EG takes place as well as a rise in

the frictional EG. Shashikumar et al. [22] performed EG analysis on the NF consisting of nanoparticles of aluminum (Al) and titanium (Ti) alloys and water as base fluid. The EG rate was reduced with augmentation in thermal conductivity (k) because of the increase in the thermal diffusion intensity.

Kumar and Mahulikar [23, 24] used numerical simulations to analyze various scaling effects on a single-phase water flow through the MC. The Fanning friction factor for the temperature-dependent density variation was found higher than that of constant property solution (CPS) due to higher radial inward velocity. Whereas for the viscosity (μ) variation, the Fanning friction factor was found prominently lower than the CPS due to a decrease in the fluid viscosity with increasing temperature. Chauhan et al. [25] executed numerical simulations for optimizing the channel geometry using the EG minimization method. It was found that the irreversibility due to conduction HT and friction got significantly affected by temperature-dependent thermal conductivity and viscosity (k(T) and μ(T)) variations, respectively.

The earlier studies discussed above pay attention only to the assessment of the EG and HT parameters, along with few studies consisting of optimization of the channels. But to the best of the author's knowledge, almost no numerical study for the channel geometry optimization has been performed with the consideration of variable NF properties. The present study consists of the following objectives: (i) to find out optimum channel diameter (D^*) corresponding to an optimum number of channels (N^*), (ii) to compare the EG of CPS and Variable property solution (VPS), (iii) to examine the effect of VF of nanoparticles on EG, and, (iv) to evaluate the irreversibility ratio.

2. Problem Formulation and Configuration

In this investigation, the problem consists of channel diameter optimization corresponding to the optimum number of channels for the least irreversibility. The computational domain has a length L and a circular cross-section of radius R_N. The water-based NF with alumina nanoparticles (Al_2O_3-water) is used as a cooling liquid; it passes through the channel of the circular constant cross-section. The total heat flow rate and total mass flow rate (m_{tot}) are 31415.926 mW and 0.180101 gm/s, respectively. Both these parameters are constant for all the cases considered in the present study while the cases and range of parameters are given in Table 1.

Table 1 Range of parameters (N, D_N, and heat flux) in the present study

Cases	N	D_N (cm)	Wall heat flux (W/cm^2)
1	1	0.10000	10.0000
2	2	0.07071	7.0711
3	5	0.04472	4.4720
4	25	0.02000	2.0000
5	100	0.01000	1.0000
6	400	0.00500	0.5000
7	625	0.00400	0.4000
8	2500	0.00200	0.2000
9	10000	0.00100	0.1000

Fig. 1 is a depiction of a fully developed (hydro-dynamically as well as thermally) steady-state laminar flow in the channel of an arbitrary circular constant cross-section of 10 μm to 1000 μm diameter, subjected to the constant wall heat flux ranging from 10^3 W/m^2 to 10^5 W/m^2, with a fixed length of 10 cm. The fluid flow is considered as single-phase. However, the working fluid is NF, but we have taken a single-phase model for the modeling of NF which needs less computational effort and is as accurate as the correlation of thermophysical properties at various nanoparticle VF. Due to the accuracy and less computational efforts, a single-phase model with thermophysical properties is the best choice for a laminar fully-developed flow [26].

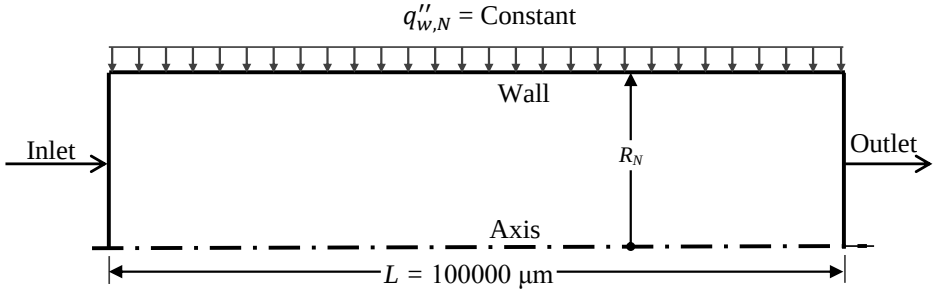

Fig. 1 Schematic diagram of circular micro-channel

Table 2 Thermophysical properties of Al_2O_3-water nanofluid [27]

	At 1% volume fraction		At 2.5% volume fraction	
Properties	Constant	Variation	Constant	Variation
Density, ρ (kg/m^3)	1016.98	1016.98	1075.18	1075.18
Specific heat, c_p (J/kg.K)	4050.63	4050.63	3754.93	3754.93
Thermal conductivity, k (W/m.K)	0.715829	0.715829	0.743896	0.743896
Dynamic viscosity, μ (Pa.s)	0.00058332	μ(T) (ref Eq. (1))	0.00119432	μ(T) (ref Eq. (2))

$$\mu(T) = \begin{Bmatrix} 1.43603444967752 - 1.85655480917592 \times 10^{-2}\, T + 9.066346037657 \\ \times 10^{-5}\, T^2 - 1.978937437 \times 10^{-7}\, T^3 + 1.6271752 \times 10^{-10} T^4 \end{Bmatrix} \quad (1)$$

$$\mu(T) = \begin{Bmatrix} 45.4142966405434 - 5.80454966169067 \times 10^{-1} T + 2.782175586943 \\ \times 10^{-3} T^2 - \ 5.9264401255 \times 10^{-6} T^3 + 4.733596 \times 10^{-9} T^4 \end{Bmatrix} \quad (2)$$

The thermophysical properties of NF at different VF of Al_2O_3 nanoparticles are taken as shown in Table 2 [27]. The working fluid for the study is water-based NF at different VF of Al_2O_3 nanoparticles with constant thermophysical properties and μ(T) as well. The derived expressions for μ(T) variation at 1% and 2.5% VF of Al_2O_3 nanoparticles in the temperature range of 298-328 K are obtained as a least-square error fourth-order polynomial fitting of data by Eq. (1) and Eq. (2), respectively [27].

3. NUMERICAL MODELING

The finite volume method is used to solve the 2-dimensional governing equations for the given initial conditions and boundary conditions. The ANSYS WORKBENCH is used for preprocessing (geometry creation and grid generation). The governing partial differential equations are solved with the help of the FLUENT solver. The further sub-sections present the governing equations, first law-based analysis, second law-based analysis, and model validation:

3.1 Governing equations

The steady-state conservation equations based on the continuous, incompressible, and 2-dimensional fluid flow in cylindrical coordinates with the μ(T) variation through the MC are following [28]:

Continuity equation:

$$\frac{v}{r}+\frac{\partial v}{\partial r}+\frac{\partial u}{\partial z}=0 \tag{3}$$

Momentum equation [Axial direction]:

$$\rho.\left(v\cdot\frac{\partial u}{\partial r}+u\cdot\frac{\partial u}{\partial z}\right)=\begin{Bmatrix}-\frac{\partial p}{\partial z}+\left[\left(\frac{\mu}{r}+\frac{\partial \mu}{\partial r}\right)\cdot\left(\frac{\partial u}{\partial r}+\frac{\partial v}{\partial z}\right)\right]+\\ \mu\cdot\left[2\left(\frac{\partial^2 u}{\partial z^2}\right)+\left(\frac{\partial^2 u}{\partial r^2}\right)+\left(\frac{\partial^2 v}{\partial r\cdot\partial z}\right)\right]+2\left(\frac{\partial \mu}{\partial z}\right)\cdot\left(\frac{\partial u}{\partial z}\right)\end{Bmatrix} \tag{4}$$

Momentum equation [Radial direction]:

$$\rho.\left(v\cdot\frac{\partial v}{\partial r}+u\cdot\frac{\partial v}{\partial z}\right)=\begin{Bmatrix}-\frac{\partial p}{\partial r}+2\left[\frac{\mu}{r}+\frac{\partial \mu}{\partial r}\right]\cdot\left(\frac{\partial v}{\partial r}\right)-\left(\frac{\mu\cdot v}{r^2}\right)+\\ \mu\cdot\left[\frac{\partial^2 v}{\partial z^2}+2\left(\frac{\partial^2 v}{\partial r^2}\right)+\frac{\partial^2 u}{\partial r\cdot\partial z}\right]+\left(\frac{\partial \mu}{\partial z}\right)\cdot\left[\frac{\partial v}{\partial z}+\frac{\partial u}{\partial r}\right]\end{Bmatrix} \tag{5}$$

In the axial and radial momentum equations, the SIMPLE algorithm is used to couple the velocity and pressure fields. Besides, the standard scheme is adopted to discretize the pressure gradient.

Energy equation:

$$\rho.c_p\left(v\cdot\frac{\partial T}{\partial r}+u\cdot\frac{\partial T}{\partial z}\right)=\left[\frac{k}{r}+\frac{\partial k}{\partial r}\right].\left(\frac{\partial T}{\partial r}\right)+k.\left(\frac{\partial^2 T}{\partial r^2}\right)+\left(\frac{\partial k}{\partial z}\right).\left(\frac{\partial T}{\partial z}\right)+k.\left(\frac{\partial^2 T}{\partial z^2}\right)+\mu.\psi \tag{6}$$

The second-order upwind scheme is used for discretizing the spatial gradients in the energy equation.

Viscous dissipation function (ψ) for the axis-symmetry condition is expressed as:

$$\psi=\begin{Bmatrix}\left[\left(\frac{\partial v}{\partial z}\right)+\left(\frac{\partial u}{\partial r}\right)\right]^2+\frac{4}{3}\begin{bmatrix}\left(\frac{\partial v}{\partial r}\right)^2+\left(\frac{v}{r}\right)^2+\left(\frac{\partial u}{\partial z}\right)^2\\ -\left(\frac{\partial v}{\partial r}\right)\cdot\left(\frac{v}{r}\right)-\left(\frac{\partial v}{\partial r}\right)\cdot\left(\frac{\partial u}{\partial z}\right)-\left(\frac{v}{r}\right)\cdot\left(\frac{\partial u}{\partial z}\right)\end{bmatrix}\end{Bmatrix} \tag{7}$$

In the above equations u, v,T, and p represent axial velocity, radial velocity, temperature, and pressure, respectively, whereas z and r represent the axial direction and radial direction, respectively.

3.2 First law of thermodynamics based analysis

The Hagen-Poiseuille equation for a hydro-dynamically fully developed velocity profile of the forced convective steady, laminar, incompressible, and Newtonian fluid flow with mean velocity (u_m) inside the channel is derived as:

$$u(r) = 2u_m\left[1 - \left(\frac{r}{R_N}\right)^2\right] \tag{8}$$

The thermally fully developed temperature profile is obtained with the help of the following equation:

$$T(r,z) = T_{0,in} + \frac{q''_{w,N}\cdot R_N}{k}\left[\left(\frac{2\alpha}{R_N\cdot u_m}\right)\left(\frac{z}{R_N}\right) + \left(\frac{r}{R_N}\right)^2 - \frac{1}{4}\left(\frac{r}{R_N}\right)^4\right] \tag{9}$$

where $T_{0,in}$ and α are inlet temperature and thermal diffusivity, respectively.

For a thermally fully developed flow with the constant wall heat flux condition, the temperature gradient along the axial direction is stated as:

$$\frac{\partial T}{\partial z} = \frac{\partial T_b}{\partial z} \tag{10}$$

where T_b is the bulk mean temperature of fluid obtained as:

$$T_b = \frac{rate\ of\ enthalpy\ flowing\ through\ a\ cross-section}{rate\ of\ \ heat\ capacity\ flowing\ through\ a\ cross-section}$$

$$T_b = \frac{2}{R_N^2 u_m}\int_0^R u(r)\cdot T(r,z)\, rdr \tag{11}$$

The governing partial differential equations (PDEs) (Eq. (3) – Eq. (6)) for the 2D computational domain are solved numerically with the help of initial and boundary conditions. These conditions are:

At the inlet (z = 0), the fully developed forced convection of Hagen-Poiseuille (Eq. (8) & Eq. (9)) is provided with temperature, $T_{0,in}$= 273 K. No entrance effects, no-slip and, no temperature-jump conditions are considered in developing the profiles. The radial velocity is taken as zero (v = 0 m/s).

At the wall (r = R), different constant wall heat flux boundary conditions (ref. Fig. 1) are applied corresponding to the tabulated cases under consideration. The slip velocity and normal flow velocity are considered as zero (non-porous rigid wall). The wall heat flux ($q''_{w,N}$) corresponding to the number of channels is calculated as:

$$q''_{w,N} = \frac{\dot{q}_{tot}}{N.(\pi.D_N.L)} \tag{12}$$

At the axis (r = 0), the differentiability of flow parameters (p, T, u) at the axis of the channels in the dimensional form is,

$$\partial p/\partial r = \partial T/\partial r = \partial u/\partial r = 0$$

At the outlet (z = L), the pressure condition is considered as atmospheric (P_{exit} = P_{atm}= 1.01325 bar). Flow transporting variables (u, v, T) are executed using the Neumann boundary condition. Their normal gradients are,

$$\partial u/\partial z = \partial v/\partial z = \partial T/\partial z = 0$$

3.3 Second law of thermodynamic based analysis

The presence of entropy in the thermal system is due to irreversibility within the system, and the EG is the measure of the magnitude of the irreversibility present in a process. The volumetric EG rate ($\dot{S}'''_{gen}$) is the sum of frictional EG rate ($\dot{S}'''_{gen,FR}$) and HT EG rate ($\dot{S}'''_{gen,FR}$), and can be obtained as [29]:

$$\dot{S}'''_{gen} = \dot{S}'''_{gen,FR} + \dot{S}'''_{gen,HT} \tag{13}$$

$$\dot{S}'''_{gen} = \frac{\mu}{T}\psi + \frac{k}{T^2}(\nabla T)^2 \tag{14}$$

$$\dot{S}'''_{gen} = \frac{\mu}{T}\psi + \frac{k}{T^2}(\nabla T)^2 \tag{15}$$

The formulation of the viscous dissipation function (Eq. (7)) is compacted to $\psi = (\partial w \partial r)^2$ by taking into account only the axial velocity. In Eq. (13), the first term on the right-hand side depends on the friction of the fluid whereas the second term depends on the HT along the finite temperature gradients. Further, the volumetric EG rate becomes,

$$\dot{S}'''_{gen} = \frac{\mu}{T}\left(\frac{\partial u}{\partial r}\right)^2 + \frac{k}{T^2}\left(\frac{\partial T}{\partial z}\right)^2 + \frac{k}{T^2}\left(\frac{\partial T}{\partial r}\right)^2 \tag{16}$$

The first-order forward difference approach is adopted to discretize the axial velocity gradient in the radial direction, the temperature gradient in the axial direction, and temperature gradient in the radial direction as:

$$\left.\frac{\partial u}{\partial r}\right|_{i,j} = \left(\frac{u_{i,j+1}-u_{i,j}}{r_{i,j+1}-r_{i,j}}\right),\ \left.\frac{\partial T}{\partial z}\right|_{i,j} = \left(\frac{T_{i+1,j}-T_{i,j}}{z_{i+1,j}-z_{i,j}}\right), and\ \left.\frac{\partial T}{\partial r}\right|_{i,j} = \left(\frac{T_{i,j+1}-T_{i,j}}{r_{i,j+1}-r_{i,j}}\right) \tag{17}$$

On substituting these gradients (Eq. (17)) in Eq. (16), and multiplying it with the total volume (= number of channels (N) × volume of a channel (V_N)) of channels, the total EG ($S_{gen,tot}$) is obtained as:

$$S_{gen,tot} = \dot{S}'''_{gen} \cdot N \cdot V_N$$

$$S_{gen,tot} = \left[\frac{\mu}{T_{i,j}}\left(\frac{u_{i,j+1}-u_{i,j}}{r_{i,j+1}-r_{i,j}}\right)^2 + \frac{k}{T_{i,j}^2}\left(\frac{T_{i+1,j}-T_{i,j}}{z_{i+1,j}-z_{i,j}}\right)^2 + \frac{k}{T_{i,j}^2}\left(\frac{T_{i+1,j}-T_{i,j}}{r_{i+1,j}-r_{i,j}}\right)^2\right] \cdot N \cdot V_N \tag{18}$$

The first, second, and third term on the right-hand side in Eq. (18) gives the frictional EG ($S_{gen,FR}$), HT EG in the axial direction ($S_{gen,HT\text{-}ax}$), and HT EG in the radial direction ($S_{gen,HT\text{-}rad}$), respectively. The sum of $S_{gen,HT\text{-}ax}$ and $S_{gen,HT\text{-}rad}$ gives the total HT EG ($S_{gen,HT}$). Further, Bejan number (Be) is calculated using,

$$Be = \frac{S_{gen,HT}}{S_{gen,tot}} \tag{19}$$

In the above equations, T is taken as local temperature i.e. $T=T_{i,j}$.

For knowing the dominance effect of frictional irreversibility over HT irreversibility in the channel, irreversibility distribution ratio (φ) is used and is given as:

$$\varphi = \frac{S_{gen,FR}}{S_{gen,HT}} = \frac{S_{gen,FR}}{S_{gen,HT-rad}+S_{gen,HT-ax}} \tag{20}$$

When, $S_{gen,FR} = S_{gen,HT}$ the diameter at intersection (D_{int}) corresponding to the number of channels is calculated. Optimum dimensions D^* corresponding to N^*occurs at the minimum value of $S_{gen,tot}$, and is obtained by the criterion,

$$\left[\partial\left(S_{gen,tot}\right)/\partial D_N\right] = 0 \tag{21}$$

3.4 Model validation

The results obtained from the numerical simulation in the CPS cases are validated by comparing with the results obtained from the explicit mathematical method used by Genić et al. [30] and Milovančević et al. [31]. Comparisons are done for pure water. The present code outcomes are in good agreement with the explicit method outcomes. The comparison of the results obtained from numerical method and explicit method is available in the preceding study performed by Chauhan et al. [15]. The model precision is ensured using six different grid systems that are 5000×25, 10000×50, 15000×75, 20000×100, 25000×125, and 30000×150. It is in the terms of the number of grids in the axial direction multiplied by the number of grids in the radial direction. The calculation of the Poiseuille number is done for each grid system and its value increases from 5000×25 to 30000×150 grid system. The increase in the Poiseuille number for the last two grids is very small whereas the computational time and effort are reasonably higher for the last grid system. Therefore, the 25000×125 grid system is selected for conducting further simulations [15].

4. RESULTS AND DISCUSSION

In this section of work, the irreversibility towards the micro-scale from macro-scale through a mini-scale for Al_2O_3-water NF at different VF with and without thermophysical property variation is presented. The effects of the μ(T) variations for different VF (1% and 2.5% VF of Al_2O_3 in base fluid water) on EG are investigated. The range of working temperature remains between 274-372 K (there is no change in the phase) in the fluid domain. So, the variations of single-phase properties are applicable.

Fig. 2 illustrates the variation in $S_{gen,HT\text{-}rad}$ along the channel diameter for CPS and VPS at different VFs. It is observed that the $S_{gen,HT\text{-}rad}$ does not play a vital role in the micro-dimension channel in comparison to the macro-dimension channel. In addition to this, the temperature gradient in the radial direction has a low value for the cases when viscosity variation is considered. At the micro-dimensions the $S_{gen,HT\text{-}rad}$ has approximately the same value for all the cases. The value of $S_{gen,HT\text{-}rad}$ experiences a sharp increase as it approaches macro-dimensions from micro-dimensions due to the lower bulk mean temperature of the fluid for bigger channel dimensions. The maximum value of $S_{gen,HT\text{-}rad}$ is for 2.5% Al_2O_3 VPS followed by CPS water, VPS water, 1% Al_2O_3 VPS, 1% Al_2O_3 CPS, and 2.5% Al_2O_3 CPS at the macro level. However, $S_{gen,HT\text{-}rad}$ is maximum for 2.5% Al_2O_3 VPS at the micro-level.

The plot between $S_{gen,HT\text{-}ax}$, and D_N is shown in Fig. 3. The observations showed that the value of $S_{gen,HT\text{-}ax}$ is insignificant in the calculation of total EG. The $S_{gen,HT\text{-}ax}$ is calculated by using $T_{i,j}$ only, as both thermal conductivity and temperature gradient in the axial direction are constant in the case of μ(T) variations. $T_{i,j}$ increases as channel dimensions are increased, so $S_{gen,HT\text{-}ax}$ decreases with an increase in the channel

dimensions. Although, $S_{gen,HT\text{-}ax}$ increases as Al_2O_3 nanoparticles VF increases and is calculated maximum for CPS or VPS at 2.5% VF of Al_2O_3 in base fluid water at micro-scale followed by CPS or VPS at 1% of Al_2O_3, and CPS or VPS of water.

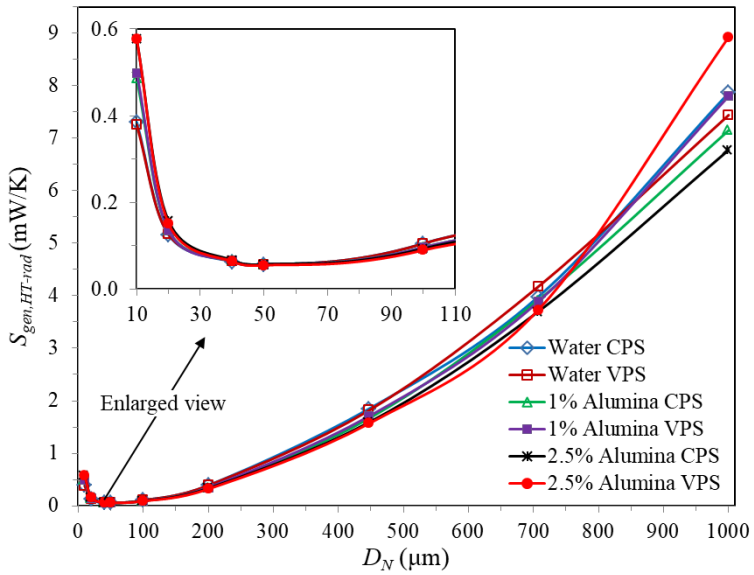

Fig. 2 The $S_{gen,HT\text{-}rad}$ versus D_N

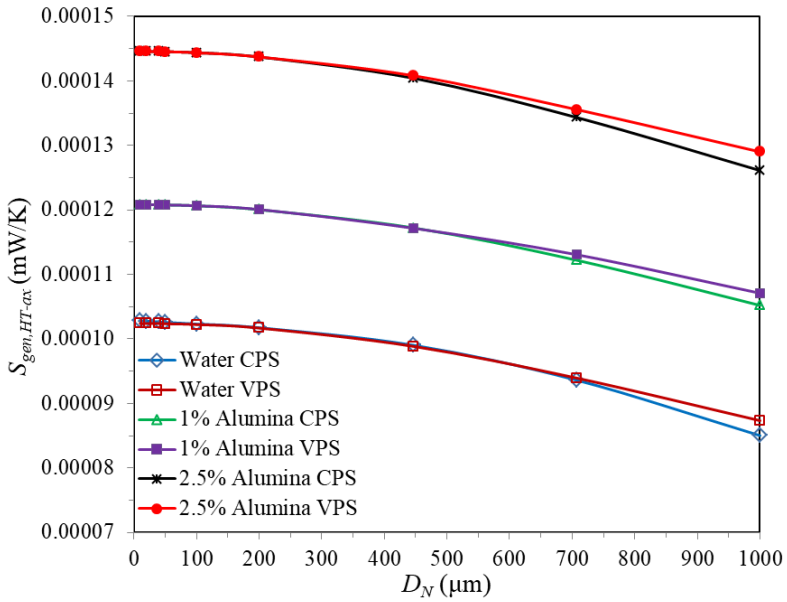

Fig. 3 $S_{gen,HT\text{-}ax}$ versus D_N

However, Fig. 4 makes it clear that $S_{gen,FR}$ plays a very important role in the calculation of total EG at micro-scale. With an increase in the channel dimensions $\mu(T_{i,j})$ decreases due to the consideration of viscosity variation. The $T_{i,j}$ value for the cases with viscosity variation is almost the same as that for the cases with CPS. But, the velocity gradient in the radial direction increases with a decrease in the channel dimensions; also this gradient is larger in the cases where viscosity variation is considered. In addition to this, the increase in particle concentration increases the frictional losses. An enlarged view of Fig. 4 demonstrates that at a higher value of VF of nanoparticles, maximum $S_{gen,FR}$ is found. It is noticed that $S_{gen,FR}$ increases drastically towards micro-dimension for both VPS and CPS. However, $S_{gen,FR}$ is maximum for the $\mu(T)$ variation due to the presence of 2.5% VF of Al_2O_3 nanoparticles in the fluid domain at micro-dimension.

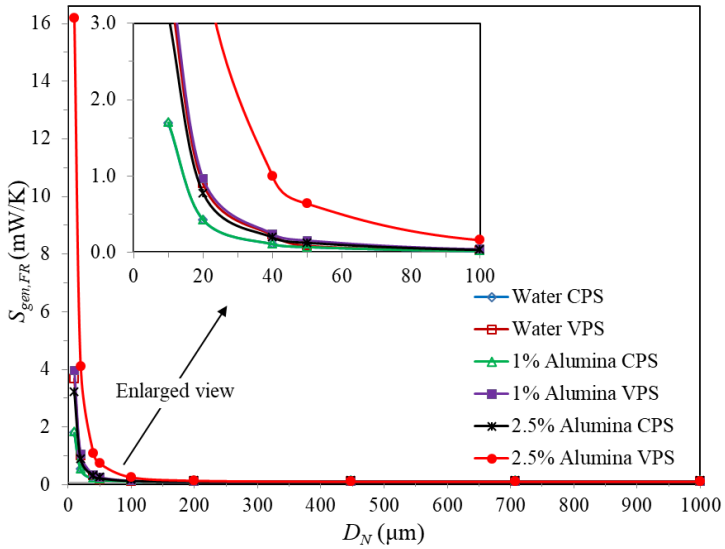

Fig. 4 $S_{gen,FR}$ versus D_N

Fig. 5 shows a valley (at minimum $S_{gen,tot}$) in the plots of $S_{gen,tot}$ for each CPS and VPS of various fluid flows from macro to micro-scale. This valley helps to calculate D^* corresponding to N^*. The VF of nanoparticles increases $S_{gen,tot}$ at the micro-level whereas it decreases $S_{gen,tot}$ at the macro level. The calculation of $S_{gen,tot}$ includes both $S_{gen,FR}$ and $S_{gen,HT}$. Therefore, $S_{gen,tot}$ is maximum investigated at micro-scale because of the greatest value of $S_{gen,FR}$ (as from Fig. 4). Therefore, it is concluded that the role of VF of nanoparticles is more significant in MC as compared to macro-channels.

Figs. 6 and 7 illustrate the variation in *Be* and φ along with D_N , respectively. For a particular diameter of MC, $S_{gen,HT}$ is found to be more for the case of CPS as compared to respective VPS. However, in macrochannel $S_{gen,HT}$ is very close to $S_{gen,tot}$ (because the value of *Be* equals to 1 approximately). The 0.5 value of *Be* indicates the equal contribution of both $S_{gen,HT}$ and $S_{gen,FR}$ in the total EG. Fig. 7 concludes the dominance effect of $S_{gen,FR}$ over $S_{gen,HT}$. The maximum dominance of $S_{gen,FR}$ is found for 2.5% VF of Al_2O_3-water NF among all the working fluids. The value of the irreversibility distribution

ratio approaches zero as the channel dimensions are increased. This is due to the dominance of HT EG at the macro-dimensions.

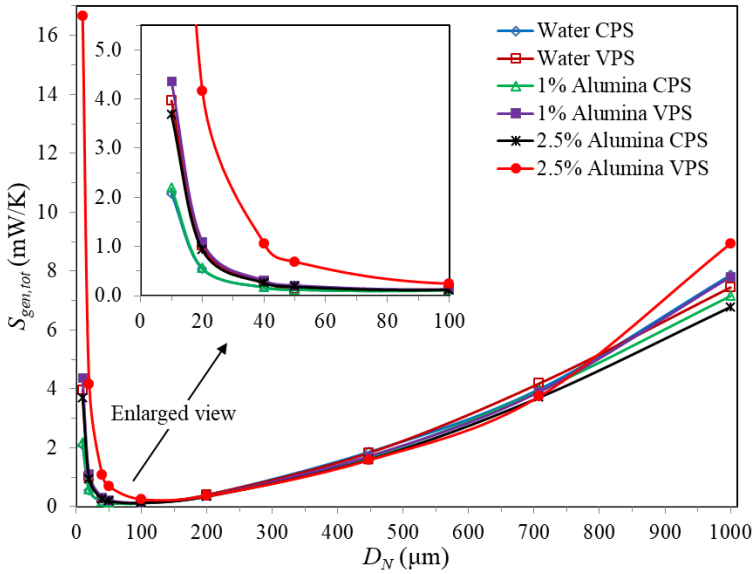

Fig. 5 $S_{gen,tot}$ versus D_N

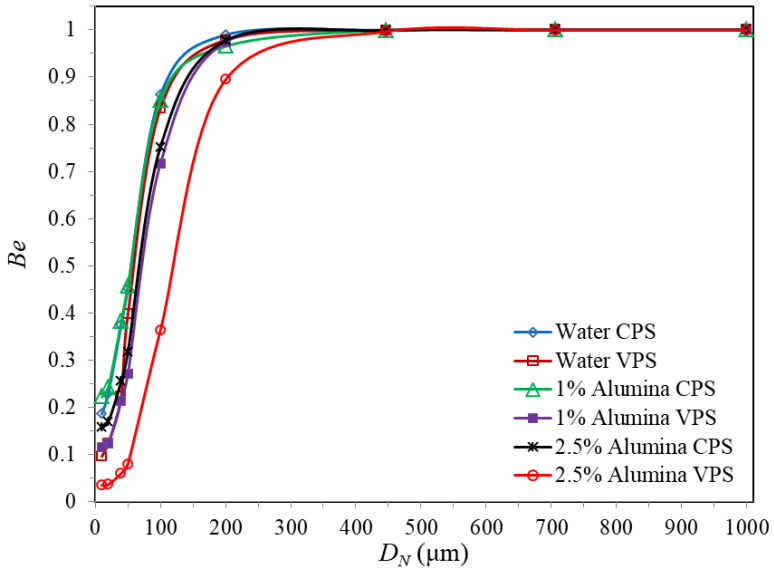

Fig. 6 *Be* versus D_N

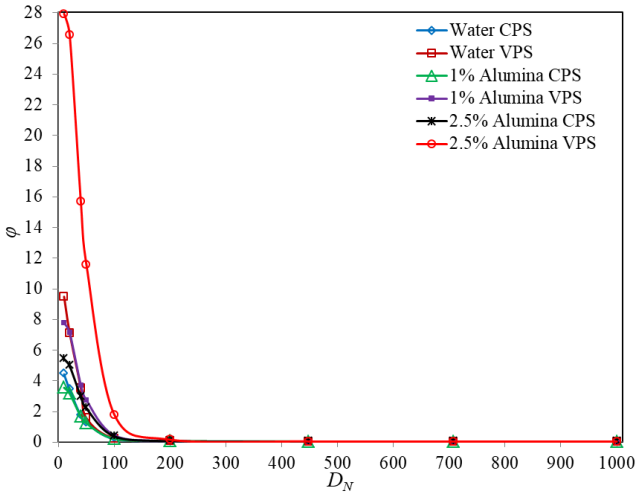

Fig. 7 φ versus D_N

5. OPTIMIZATION

The problem undertaken in the present work is to optimize the channel diameter by minimizing the total EG rate, given by Eq. (21) for the best possible overall performance of the MC heat sink. Figs. 8, 9, and 10 illustrate the plots of variation in S_{gen} for CPS and VPS along with channel diameter for water, 1% Al_2O_3-water NF, and 2.5% Al_2O_3-water NF, respectively. These plots depict that $S_{gen,HT}$ and $S_{gen,FR}$ intersect (at $S_{gen,HT} = S_{gen,FR}$) each other at a point. This helps to determine the values of D_{int} for both CPS and VPS.

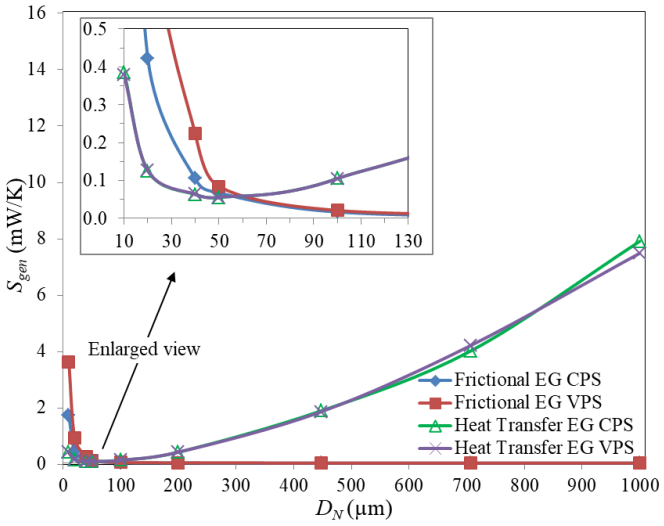

Fig. 8 S_{gen} versus D_N for water

For a better view of the intersection zone, an enlarged view is shown in the respective figures (Figs. 8-10). The results show that as VF of Al_2O_3 nanoparticles increase in the base fluid, D_{int} shifts toward the right side in the plot for both CPS and VPS because of a faster rate of the friction change than that of HT change. Additionally, it is also found that at a particular VF (1% or 2.5%) of Al_2O_3 nanoparticles in water, D_{int} has more value for VPS as compared to CPS.

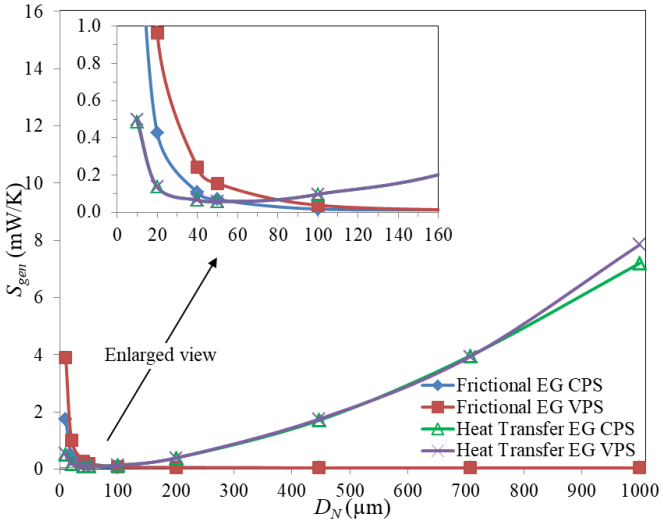

Fig. 9 S_{gen} versus D_N for 1% Al_2O_3 nanoparticle concentration nanofluid

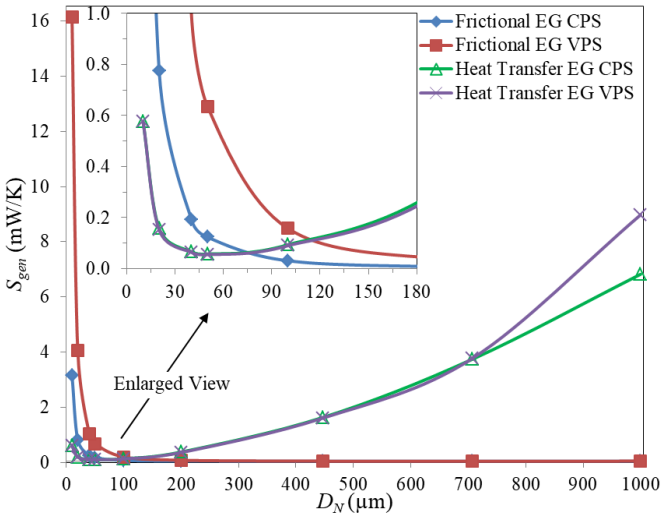

Fig. 10 S_{gen} versus D_N for 2.5% Al_2O_3 nanoparticle concentration nanofluid

Table 3 shows N (actual) corresponding to D_{int}, and D^* corresponding to N^* (a natural number) for various VF of Al_2O_3 nanoparticles in water. D^* is calculated maximum for 2.5% Al_2O_3-water NF with μ(T) variation followed by 1% Al_2O_3-water NF with μ(T) variation, 2.5% Al_2O_3-water NF with CPS, and 1% Al_2O_3-water NF with CPS. From Fig. 5 and Table 3 it can be interpreted that for the flow of NFs, the lowest total EG is for the case of 1% VF of Al_2O_3 nanoparticles with CPS. So, 58.72 μm is the optimum diameter of the channel under the considered condition and NF flow.

Table 3 Optimum channel diameter corresponding to N^*

Nanofluids	N (actual)	D_{int} (μm)	N^* (natural number)	D^*(μm)
1% Al_2O_3-water NF CPS	290.18	58.70	290	58.72
1% Al_2O_3-water NF μ(T)	155.16	80.28	155	80.32
2.5% Al_2O_3-water NF CPS	175.34	75.52	175	75.59
2.5% Al_2O_3-water NF μ(T)	75.30	115.24	75	115.47

6. CONCLUSIONS

In this numerical study, the channel geometry (macro to micro-scale) is optimized for the flow of the NF with different VF using irreversibility analysis. Besides, the effects of μ(T) variation on HT EG, frictional EG, and total EG are also analyzed. The study concluded that:

1. The variations in $S_{gen,HT\text{-}ax}$ and $S_{gen,HT\text{-}rad}$ are not found significant but they increase with increment in the VF of Al_2O_3 nanoparticles.

2. The $S_{gen,FR}$ drastically increases as the VF of Al_2O_3 nanoparticles increase. Therefore, it has a major role in calculating $S_{gen,tot}$ at micro-dimension. This increment in $S_{gen,FR}$ is due to the increment in the flow friction with the rising VF of the nanoparticles.

3. At micro-scale, the μ(T) variation also does not have a significant impact on the value of $S_{gen,HT\text{-}ax}$ and $S_{gen,HT\text{-}rad}$ because of low temperature in the flow domain in comparison to the macro-scale. However, $S_{gen,\,FR}$ increases rapidly at micro-scale because of a larger velocity gradient in the radial direction.

4. When μ(T) variation effect is considered, $S_{gen,tot}$ is found maximum for 2.5% VF of Al_2O_3 nanoparticles among all the CPS and VPS for various kinds of working fluids.

5. At a particular VF (1% or 2.5%) of Al_2O_3 nanoparticles in water-based NF, D_{int} has more value for VPS comparing to CPS because of a higher velocity gradient in the radial direction when viscosity variation is considered.

6. The calculated value of D^* is maximum for 2.5% Al_2O_3-water NF with μ(T) variation followed by 1% Al_2O_3-water NF with μ(T) variation, 2.5% Al_2O_3-water NF with CPS, and 1% Al_2O_3-water NF with CPS.

REFERENCES

1. Xie, J., Amano, R.S., 2004, *Numerical simulation of two-phase flow in microchannel*, IEEE Ninth Intersociety Conference on Thermal and Thermomechanical Phenomena in Electronic Systems (IEEE Cat. No. 04CH37543), 2, pp. 679-686.
2. Han, S., Gongnan, X., Chi-Chuan, W., 2020, *Thermal performance and entropy generation of novel X-structured double layered microchannel heat sinks*, Journal of the Taiwan Institute of Chemical Engineers., 111, pp. 90-104.

3. Oztop, H.F., Abu-Nada, E., 2008, *Numerical study of natural convection in partially heated rectangular enclosures filled with nanofluids*, International Journal of Heat and Fluid Flow, 29(5), pp. 1326-36.
4. Tayebi, T., Öztop, H.F., 2020, *Entropy production during natural convection of hybrid nanofluid in an annular passage between horizontal confocal elliptic cylinders*, International Journal of Mechanical Sciences, 171, 105378.
5. Zúñiga-Cerroblanco, J.L., Gonzalez-Valle, C.U., Lorenzini-Gutierrez, D., Hernandez-Guerrero, A., Cervantes de Gortari, J., 2016, *Heat sink performance improvement by way of nanofluids*, Proceedings of the ASME 2016 Heat Transfer Summer Conference collocated with the ASME 2016 Fluids Engineering Division Summer Meeting and the ASME 2016 14th International Conference on Nanochannels, Microchannels, and Minichannels, Washington, DC, USA, 2.
6. Kumar, K., Kumar, R., Bharj, R.S., Mondal, P.K., 2021, *Irreversibility analysis of the convective flow through corrugated channels: a comprehensive review*, The European Physical Journal Plus, 136(4), pp. 1-40.
7. Bejan, A., 1980, *Second law analysis in heat transfer*, Energy, 5(8-9), pp. 720-732.
8. Kumar, K., Kumar, R, Bharj, R.S., 2020, *Entropy generation analysis due to heat transfer and nanofluid flow through microchannels: a review*, International Journal of Exergy, 31(1), pp. 49-86.
9. Chen, K., 2004, *Second- law analysis and optimization of microchannel flows subjected to different thermal boundary conditions*, International Journal of Energy Research, 29(3), pp.249-263.
10. Bejan, A., 1995, *Entropy Generation Minimization: The Method of Thermodynamic Optimization of Finite-Size Systems and Finite-Time Processes*, CRC Press, Boca Raton.
11. Bejan, A., 2002, *Fundamentals of exergy analysis, entropy generation minimization, and the generation of flow architecture*, International Journal of Energy Research, 26(7), pp. 545-565.
12. Kumar, R., Mahulikar, S.P., 2015, *Effect of temperature-dependent viscosity variation on fully developed laminar microconvective flow*, International Journal of Thermal Sciences, 98, pp. 179-191.
13. Rastogi, P., Mahulikar, S.P., 2018, *Entropy generation in laminar forced convective water flow due to overloading toward the microscale*, ASME Journal of Energy Resources Technology, 140(8), 082002.
14. Rastogi, P., Mahulikar, S.P., 2018, *Optimization of micro-heat sink based on theory of entropy generation in laminar forced convection*, International Journal of Thermal Sciences, 126, pp. 96-104.
15. Chauhan, P.R., Kumar, R., Bharj, R.S., 2019, *Optimization of the circular microchannel heat sink under viscous heating effect using entropy generation minimization method*, Thermal Science and Engineering Progress, 13, 100365.
16. Kumar, K., Kumar, R. Bharj, R.S., 2020, *Circular microchannel heat sink optimization using entropy generation minimization method*, Journal of Non-Equilibrium Thermodynamics, 45(4), pp. 333-342.
17. Heshmatian, S., Bahiraei, M., 2017, *Numerical investigation of entropy generation to predict irreversibilities in nanofluid flow within a microchannel: effects of Brownian diffusion, shear rate and viscosity gradient*, Chemical Engineering Science, 172, pp. 52-65.
18. Bianco, V., Scarpa, F., Tagliafico, L.A., 2018, *Numerical analysis of the Al_2O_3-water nanofluid forced laminar convection in an asymmetric heated channel for application in flat plate PV/T collector*, Renewable Energy, 116, pp. 9-21.
19. Manay, E., Akyürek, E.F., Sahin, B., 2018, *Entropy generation of nanofluid flow in a microchannel heat sink*, Results in Physics, 9, pp. 615-624.
20. Bianco, V., Marchitto, A., Scarpa, F., Tagliafico, L.A., 2019,*Numerical investigation on the forced laminar convection heat transfer of Al_2O_3-water nanofluid within a three-dimensional asymmetric heated channel*, International Journal of Numerical Methods for Heat & Fluid Flow, 29(3), pp. 1132-1152.
21. Alfaryjat, A.A., Dobrovicescu, A., Stanciu, D., 2019, *Influence of heat flux and Reynolds number on the entropy generation for different types of nanofluids in a hexagon microchannel heat sink*, Chinese Journal of Chemical Engineering, 27(3), pp. 501-513.
22. Shashikumar, N.S., Gireesha, B.J., Mahanthesh, B., Prasannakumara, B.C., Chamkha, A.J., 2019, *Entropy generation analysis of magneto-nanoliquids embedded with aluminium and titanium alloy nanoparticles in microchannel with partial slips and convective conditions*, International Journal of Numerical Methods for Heat & Fluid Flow, 20(10), pp. 3638-3658.
23. Kumar, R., Mahulikar, S.P., 2018, *Physical effects of variable thermophysical fluid properties on flow and thermal development in micro-channel*, Heat Transfer Engineering, 39(4), pp. 374-390.
24. Kumar, R., Mahulikar, S.P., 2020, *Heat transfer characteristics of water flowing through micro-tube heat exchanger with variable fluid properties*, Journal of Thermal Analysis and Calorimetry, 140, pp. 1919–1934.
25. Chauhan, P.R., Kumar, K., Kumar, R., Rahimi-Gorji, M., Bharj, R.S., 2020, *Effect of thermophysical property variation on entropy generation towards micro-scale*, Journal of Non-Equilibrium Thermodynamics, 45(1), pp. 1-7.

26. Wen, D., Ding, Y., 2004, *Experimental investigation into convective heat transfer of nanofluids at the entrance region under laminar flow conditions*, International Journal of Heat and Mass Transfer, 47(24), pp. 5181-5188.
27. Hussein, A.M., Bakar, R.A., Kadirgama, K., Sharma, K.V., 2013, *Experimental measurement of nanofluids thermal properties*,International Journal of Automotive and Mechanical Engineering, 7, pp. 850-863.
28. Kumar, R., Mahulikar, S.P., 2017, *Numerical re-examination of Chilton–Colburn analogy for variable thermophysical fluid properties*, ASME Journal of Heat Transfer, 139(7), 071701.
29. Bejan, A., 1982, *Entropy Generation through Heat and Fluid Flow*, New York: Wiley.
30. Genić, S., Jaćimović, B., Petrovic, A., 2018, *A novel method for combined entropy generation and economic optimization of counter-current and co-current heat exchangers*, Applied Thermal Engineering, 136, pp. 327-334.
31. Milovančević, U.M., Jaćimović, B.M., Genić, S.B., El-Sagier, F., Otović, M.M., Stevanović, S.M., 2019, *Thermoeconomic analysis of spiral heat exchanger with constant wall temperature*, Thermal Science, 23(1), pp. 401-410.